Vitamin B9 as a new eco-friendly corrosion inhibitor for copper in 3.5% NaCl solution

Hubert Kwiatkowski[a] (s189130@student.pg.edu.pl)

Stefan Krakowiak[a] (stekrako@pg.edu.pl)*

Łukasz Gaweł[a] (lukasz.gawel@pg.edu.pl)

*corresponding author

Family names underlined.

[a]Department of Electrochemistry, Corrosion and Materials Engineering, Faculty of Chemistry, Gdansk University of Technology, Narutowicza Str. 11/12, 80-233 Gdansk, Poland

Highlights:

- Sodium folate was found as an effective copper corrosion inhibitor in chloride media
- Effect of temperature, time and concentration on the inhibitor efficiency was studied
- Various measurement methods were applied to investigate the nature of inhibiting action

Abstract: Folic acid salt (sodium folate) was studied as an eco-friendly and non-toxic copper corrosion inhibitor in 3.5% NaCl solution. Electrochemical impedance spectroscopy, polarization resistance and weight-loss measurements show that the inhibitor efficiency increases with concentration (the highest value- approx. 96% was reported for the solution containing 16 mM sodium folate after 24 h). EIS data and Tafel plots indicate that sodium folate is a barrier, mixed-type (with predominant cathodic character) inhibitor. Inhibitor efficiency decreases with temperature, which suggests that adsorption has physical character rather than chemical one - adsorption free energy calculated using the Langmuir model is consistent with this statement. Activation energy determined from the Arrhenius plot increases as a result of inhibitor presence. Efficiency of the inhibitor increases systematically during the first 12 hours of immersion. Potential chemical changes in sodium folate solution were investigated using UV-VIS spectroscopy. Furthermore, copper surface after immersion in the presence and absence of inhibitor was characterized with scanning electron microscopy, energy-dispersive X-Ray spectroscopy and microscopic photographs.

Keywords: folic acid, vitamin B9, green corrosion inhibitor, adsorption, copper

1. Introduction

Copper is one of the most widely used metals. Its global production systematically increases and in 2022 reached 48000 metric tons [1]. Because of their numerous useful properties, such as good thermal and electrical conductivity, relatively high corrosion resistance and malleability, copper and its alloys are commonly applied in many fields, for instance pipelines, heat exchangers, ship building, electronics and sea water desalinations [2]. When used in the marine industry, copper is exposed to aggressive chloride ions and the occurring corrosion process can lead to costly damages, hence appropriate protection of the metal elements (for example by using corrosion inhibitors) is required [3].

The most important group of copper corrosion inhibitors in chloride solutions consists of azole compounds. For instance, inhibiting effects of benzotriazole [4], indazole derivatives [5], 2-mercaptobenzothiazole [6], tetrazole derivatives [7], 1,2,4-triazole derivative [8] and 1-hydroxybenzotriazole [9] have been described. Schiff bases have also been extensively studied in this field [10, 11]. In the last few years non-toxic and environmentally friendly inhibitors have been gaining scientists' attention. In addition to synthetic compounds (for example amino acids [12, 13], phytic acid [14] or vanillin derivative [15]), also natural products have been reported as copper green corrosion inhibitors in chlorides. In this case, blackberry leaf [16], olive leaf [17], and turnip peel [18] extracts, chitosan [19], propolis extract [20] or inhibitor synthesized from coffee bagasse oil [21] can be given as examples. However, in comparison to steel, the number of green corrosion inhibitors for copper is rather small and needs to be increased.

Vitamin B9 (folate) is a general term used for folic acid and some related compounds [22]. It occurs naturally in plant leaves (lat. *folium*- leave), moreover, dietary sources of vitamin B9 are green vegetables, rice, corn and liver. It is a micronutrient that plays an important role in human metabolism [23]. Lack of folate increases the risk of neural tube birth defects, cognitive and psychiatric dysfunction, cancer, and cardiovascular disease. Natural forms of folate are relatively unstable; hence, there is a need, mainly concerning pregnant women, to supplement synthetic folic acid [22]. In many countries, bread and grain products are fortified with this compound [24], furthermore, it is used as a typical nutritional supplement and in cosmetics industry [25]. A wide spectrum of nanoparticles with potential applications in different fields, such as cancer nanotechnology [26, 27] or drug delivery [28, 29], have been synthesized using folic acid. Importantly it has also been described as a corrosion inhibitor for steel in chloride solutions (folic acid itself [30] and as part of a phosphonate-based system [31]), phosphoric acid [32] and washing water from crude oil [33]. Potassium folate inhibiting action for copper in Na_2SO_4 has been also reported [34]. Some authors have suggested that the presence of folic acid in plant extracts is responsible for the observed inhibiting effects [35–37].

The non-toxic and environmentally friendly nature of vitamin B9, the presence of potentially donor nitrogen atoms and π-electron systems in its structure, and the results mentioned above suggest that it will act as a green corrosion inhibitor for copper in chloride solutions. Due to the low solubility of folic acid in neutral and acidic environments (between 10^{-4} and 10^{-5} M in slightly acidic NaCl solutions at 298 K [38]), it was used as a salt - sodium folate (Na_2HFol,

Figure 1

Figure 1). The aim of this study was to examine its efficiency under different conditions and explain the mechanism of inhibiting phenomenon using various measurement techniques.

2. Material and methods

2.1. Samples and solutions

The working electrodes were made from a copper rod (99.96% Cu, 0.02% Zr, 0.01% Co, trace

amounts of Zn, Sn and Pb, confirmed by X-Ray Fluorescence with Bruker S1 Titan analyzer), which was cut and embedded in epoxy resin (the area exposed to the solution was 1 cm^2). Before each measurement, the electrodes were polished using emery paper (in sequence 240, 600, 1200 and 2500 grit size), rinsed with demineralized water, degreased with acetone and air-dried. Specimens used for weight-loss method test were rectangular (approx. 20x50 mm) coupons (99.97% Cu, 0.02% Co, trace amounts of Fe, Zn, Sn and Pb, confirmed by X-Ray Fluorescence). Sodium folate solutions were made by adding a suitable amount of folic acid and sodium hydroxide (molar ratio 1:2) to 3.5%(w/w) NaCl solution prepared before.
All reagents and chemicals used were of analytical grade.

2.2. Electrochemical measurements

Electrochemical measurements were carried out using a three-electrode cell (the working electrode, saturated calomel electrode (SCE) as a reference and the platinum mesh as an auxiliary electrode), Gamry Reference 600 potentiostat-galvanostat and Gamry software. The experiments were carried out in a thermostat at 298 K (if not specified otherwise).
Electrochemical impedance spectroscopy (EIS) measurements were performed in the frequency range from 10000 to 0.1 Hz (AC perturbation voltage 10 mV/ms, 8 points/decade). EIS data were analyzed using ZSimpWin software. Inhibitor efficiency (η) values were calculated using the following formula [5, 13]:

$$\eta = \frac{R_{ct}^{inh} - R_{ct}^{0}}{R_{ct}^{inh}} * 100 \qquad \text{Eq. 1}$$

where R_{ct}^{0} and R_{ct}^{inh} are the charge-transfer resistance values obtained without or with inhibitor, respectively, under the same conditions.
Linear polarization was performed in the potential range ±0.02 V vs. open circuit potential (scan rate 0.125 mV/s). Polarization resistance values (R_p), given by the equation:

$$R_p = \left(\frac{dE}{di}\right)_{Ecorr} \qquad \text{Eq. 2}$$

where E stands for the potential, E_{corr}- corrosion potential, i- exchange current density, were determined by estimating the slopes of the obtained polarization curves near to i=0 [39,40]. Moreover, inhibitor efficiency values were calculated using the formula [41]:

$$\eta = \frac{R_{p}^{inh} - R_{p}^{0}}{R_{p}^{inh}} * 100 \qquad \text{Eq. 3}$$

where R_p^{inh} and R_p^{0} stand for polarization resistance with or without inhibitor, respectively.
Potentiodynamic polarization measurements [42] were carried out in the potential range ±0.250 V vs. open circuit potential (scan rate 1 mV/s).
To ensure repeatability, experiments were carried out 2-3 times.

2.3. Weight-loss measurements

Copper coupons were pickled in 63% nitric acid solution for 10 seconds, rinsed carefully with demineralized water and air-dried, then weighed three times on analytical balance and immersed in 3.5% NaCl solutions with or without Na_2HFol in different concentrations. After 20 days of immersion at room temperature, the specimens were removed from the solutions, rinsed with demineralized water, pickled for 10 minutes in 10% sulfuric acid solution to remove corrosion products, rinsed with demineralized water, air-dried and weighed three times again [43]. The weight of each specimen after immersion and removal of corrosion products was compared to the value before and inhibitor efficiency values were calculated using the following formula:

$$\eta = \frac{\frac{\Delta m_0}{S_0} - \frac{\Delta m_{inh}}{S_{inh}}}{\frac{\Delta m_0}{S_0}} * 100 \qquad \text{Eq. 4}$$

where Δm_0, Δm_{inh} are differences between specimen mass before and after immersion in the solution without or with inhibitor respectively and S_0, S_{inh} stand for corresponding coupons' surface areas.

2.4. UV-VIS spectroscopy

The measurements were performed on Merck Spectroquant Prove 100 UV-VIS spectrophotometer in the wavelength range from 200 to 1100 nm, using 10x10 mm quartz cuvette and demineralized water as "zero" solution. All solutions were diluted 25 times before the measurement. Copper coupons immersed in the solutions were prepared using the procedure described for weight-loss measurements.

2.5. Surface analysis

Cylindric specimens made from the copper rod were polished using emery paper (in sequence 240, 600, 1200 and 2500 grid size), rinsed with demineralized water and immersed in 3.5% NaCl solution without or with Na_2HFol at a concentration of 12 mM. After this time, the specimens were removed, rinsed with demineralized water, dried under reduced pressure and analyzed. Microscopic photographs were taken using inverted microscope with episcopic illumination Nikon ECLIPSE MA200. Scanning electron microscope (SEM) images and energy-dispersive X-Ray (EDX) spectra were obtained with Hitachi S-3400N microscope with ThermoFisher Scientific EDS detector. EDX measurements were repeated 3-4 times at different places of each specimen to ensure the validity of the obtained results.

3. Results and discussion

3.1. Effect of concentration

3.1.1. Electrochemical impedance spectroscopy

The first method applied to examine efficiency of Na_2HFol inhibiting action in different concentrations was electrochemical impedance spectroscopy. To ensure the stability of the investigated system, all measurements were carried out after 24h of immersion of the working electrode in the solution with or without appropriate Na_2HFol concentration. At the center of the obtained impedance spectra in the Nyquist projection (reactance Z_{imag} vs. resistance Z_{real}, Figure 2a), a part of a semicircle, which can be attributed to the charge-transfer resistance and the electrical double layer capacitance is observed. The diameter of the semicircle increases significantly with the concentration of Na_2HFol – it indicates an increase in charge-transfer resistance and deceleration of the corrosion process. At lower frequencies one can find the straight line corresponding to the Warburg impedance. For higher concentrations of Na_2HFol it disappears, presumably as a result of the adsorption of folate and blocking the diffusion of reactants to and from the electrode. Moreover, at high frequencies, a part of a smaller semicircle corresponding to the resistance and constant phase element of the film on the electrode surface also occurs [39, 40]. The spectra obtained for the blank solution and the solution with the lowest concentration of Na_2HFol were analyzed using an electrical equivalent circuit presented in Figure 3a, whereas the spectra measured for higher Na_2HFol concentrations were fitted to the circuit shown in Figure 3b. The elements of the circuits are the solution resistance (R_s), film resistance (R_f) and constant phase element (Q_1, n_1), charge-transfer resistance (R_{ct}) and constant phase element corresponding to the electrical double layer capacitance (Q_2, n_2). The first circuit contains also Warburg diffusion element [41, 42]. The calculated values of all parameters listed above and χ^2 values representing the quality of model fitting are presented in Table 1. R_s values

are only slightly lower in the presence of Na_2HFol (conductivity of the solution depends rather on NaCl concentration than the concentration of large folate anions). The film capacitance (C_f) is given by the equation [48]:

$$C_f = \frac{F^2 S}{4RT} \quad \text{Eq. 5}$$

where F is Faraday's constant, S- electrode surface exposed to the solution, R- gas constant and T- absolute temperature. Due to the electrode surface imperfection, C_f is represented by constant phase element Q_1, which decreases with Na_2HFol concentration. This can be explained by covering the electrode surface with folate and reducing "active" surface area S. Furthermore, R_f increases with Na_2HFol concentration as a result of adsorbing a higher amount of folate anions on the surface. The electrical double layer capacitance, described by the formula [48]:

$$C_{dl} = \frac{\varepsilon_0 \varepsilon S}{d} \quad \text{Eq. 6}$$

where ε_0 is vacuum permittivity, ε- local dielectric constant, d- electrical double layer thickness, is represented by constant phase element Q_2. The decrease in its value can be explained by a combination of three effects caused by the adsorption process: replacing water molecules adsorbed on the electrode surface by folate, which results in ε decrease, reducing S value as described before, and some changes in the electrical double layer geometry, leading to an increase in its thickness. Charge transfer resistance increases with Na_2HFol concentration- it results in the increase in inhibitor efficiency, which reaches a maximum value of 95.8% for 16 mM. Additionally, W value for the solution containing 4 mM Na_2HFol is lower than that for the blank solution, which confirms that the addition of sodium folate limits the mass transport process [49]. All these results indicate that Na_2HFol inhibits corrosion of copper by adsorption on its surface and diffusion barrier formation.

3.1.2. Linear polarization resistance

To verify the results obtained by EIS, linear polarization experiments were performed under the same conditions. Polarization resistance (R_p) values are presented in Table 2. It can be easily observed that R_p increases with inhibitor concentration. The obtained inhibitor efficiency values are in a good agreement with those calculated from EIS data. Polarization curves (potential E vs. exchange current density i) are presented in Figure 2b.

3.1.3. Potentiodynamic polarization

Potentiodynamic polarization is another method commonly used in corrosion inhibitor efficiency studies. All measurements were carried out after 24 h conditioning of the experimental setup. Analyzing the obtained curves (potential E vs. current density module |i|, **Error! Reference source not found.**c), one can easily notice that the shape of cathodic branches indicates diffusion control of the oxygen reduction process. For lower E values (between -0.35 and -0.40 V vs. SCE), a current increase is observed. It can be explained by the hydrogen evolution process, which remains under activation control [9]. Moreover, for the solutions containing inhibitor, strong concentration polarization is also visible on anodic branches and becomes more pronounced with Na_2HFol concentration increase. This can be interpreted as further proof of diffusion barrier formation on the electrode surface by inhibitor molecules. The visible deformation of the anodic branches may be attributed to the complexity of the copper oxidation process (at different potentials different reactions can occur with various rates) and/or inhibitor desorption. As a result of the fact that the investigated processes are not under pure activation control, cathodic and anodic (besides the measurement for the blank solution) branches do not show a clearly defined Tafel region; hence, Tafel curves extrapolation is not a suitable method for determining the corrosion current - the obtained values might be incorrect. However, visual assessment may lead to the observation that the current decreases

with inhibitor concentration increase [6, 47]. Nevertheless, it is worth noticing that the corrosion potential shifts down slightly with inhibitor concentration increase - regarding that in the solutions containing Na_2HFol both cathodic and anodic branches are changed in comparison to the blank solution, it can be stated that sodium folate acts as a mixed-type inhibitor, with predominant cathodic character [51].

3.1.4. Weight-loss method

Efficiency of the inhibiting action under long-term exposure conditions can be different from that after short-term immersion due to several factors. The simplest way to obtain this value is the weight-loss method. After 20 days of immersion, the surface of the specimen exposed to the solution without Na_2HFol was visibly changed and covered with red corrosion products. After removing it from the solution, the color of formed film slowly changed to grey-blue (see Supplementary material), probably as a result of the oxidation of Cu_2O to $Cu(OH)_2$ and CuO with oxygen from the air [3]. The surfaces of specimens exposed to the solution with inhibitor seemed to be uncorroded; however, their appearance is slightly different for each concentration, which also indicates the effect of inhibitor concentration on its efficiency. It can be noticed that η values increase with inhibitor concentration but are noticeably lower than those obtained in electrochemical measurements after short-time immersion. The main reason for this is the formation of the corrosion products layer on the specimen immersed in blank solution. It plays a protective role and causes an increase in copper corrosion resistance, hence Δm_0 cannot be treated as the value for completely unprotected copper as in the case of previous measurements. Simultaneously, the film of corrosion products is not observed on the specimens exposed to the solution containing inhibitor. Therefore, it must be emphasized that a lower value of the calculated inhibitor efficiency does not mean that inhibitor adsorption decreased to the same extent. The second cause of the η decrease in time are potential chemical changes in the solution, which were also investigated in the further part of the paper (see Chapter 3.4). Different chemical compositions of used copper specimens can also affect the adsorption process, but in comparison to the factors described above its impact is rather deniable.

3.1.5. Adsorption isotherm

The most common method for determination of the adsorption isotherm for corrosion inhibitors is based on the statement that the surface coverage coefficient θ is equal to the inhibitor efficiency η. For the studied system, η values obtained from EIS were used to fit some adsorption isotherm models: Langmuir, Temkin, Freundlich, Frumkin, Flory-Huggins, and El-Awady [52-54] using linear relationships presented in Table 3. For the Langmuir model, the coefficient of determination (R^2) reaches the highest value, therefore, the further calculations were performed in relation to this model. Its graphical representation is shown in Figure 4 (other figures are available in Supplementary material). The equilibrium constant of the adsorption process (K) was extracted from the intercept of the obtained linear function and standard adsorption free energy (ΔG^o) was calculated using the formula [13, 54]:

$$\Delta G^o = -RTln(55.5K) \qquad \text{Eq. 7}$$

where R stands for ideal gas constant (8.314 J/(mol K)) and 55.5 is approximated water molar concentration in diluted solutions. The obtained ΔG^o value is -27.4 kJ/mol. It is usually assumed that ΔG^o higher than -20 kJ/mol indicates that the physisorption occurs, while values more negative than -40 kJ/mol are typical for the chemisorption [52]. Referring to this, it can be stated that Na_2HFol adsorption is mixed-type, possibly with predominant physical character, however, it should be noted that the assumption about the equality of θ and η is approximate (the exemplary reason of the possible deviation from this model is the formation of protective corrosion products layer on the metal surface). Moreover, the mentioned limit ΔG^o values should be regarded as indicative only and sometimes may lead to the incorrect conclusions [56].

Therefore, some experiments need to be done to better understand the nature of occurring adsorption process (see Chapter 3.3).

3.2. Effect of time

Changes in the investigated system during the first 12 hours of immersion in the blank solution and the solution containing 12 mM Na_2HFol were studied using electrochemical impedance spectroscopy. The spectra were measured at 1-hour intervals and are presented in Figure 5a. Capacitive loops measured for the inhibited system have bigger diameters than obtained for the blank solution. Furthermore, straight line corresponding to Warburg diffusion element is not visible in the presence of Na_2HFol. Selected EIS data are listed in Table 4 (all data are available in Supplementary material). R_{ct} value (Figure 5b) for copper electrode immersed in blank solution firstly decreases from over 1000 ohms to about 700 ohms, which corresponds to the initiation of corrosion process. After 8 hours of immersion, it begins to increase slightly, probably as a result of the formation of protective layer of corrosion products. In the solution containing inhibitor, R_{ct} value (Figure 5b) increases significantly during the first 8 hours. Further changes are smaller, but also lead to R_{ct} growth. This fact can be explained by progressing adsorption of inhibitor on Na_2HFol surface, which corresponds also to the decrease in Q_1 and Q_2 values. R_{ct} values are remarkably higher in the presence of inhibitor, the efficiency calculated from eq. 3 (Figure 5b) increases in time during the first 8 hours of immersion and then remains almost unchanged. It is worth noticing that n_1 values are closer to 1 for the solutions containing inhibitor - it indicates that species on the electrode surface are more organized than in the case of blank solution.

3.3. Effect of temperature

3.3.1. Electrochemical impedance spectroscopy

To determine how temperature affects the efficiency of Na_2HFol inhibiting action, two series of impedance measurements were performed: one for the blank solution and the second for the solution containing 16 mM inhibitor, at 25, 40, 60 and 80°C in each case. The measured spectra (Figure 6a) are similar to those obtained in previous measurements. Analyzing the calculated data (Table 5), one can notice that, as might be assumed, R_s decreases with temperature. In both solutions R_{ct} value decreases with temperature, which indicates that the corrosion process speeds up; moreover, the values obtained for the solution containing inhibitor are higher. The inhibitor efficiency given by Eq. 3 decreases with temperature - the decrease in R_f value and increase in Q_1 and Q_2 suggest that it is a result of smaller adsorption of inhibitor on the electrode surface. These facts clearly indicate that the adsorption process has a physical (or mixed with predominant physical) character [57]. Furthermore, possible chemical changes in the solution as a result of exposure to relatively high temperatures are another important factor that can affect the adsorption process and inhibitor efficiency (see Chapter 3.4).

3.3.2. Arrhenius plot

For small overpotentials, the exchange current (i) is related to charge-transfer resistance with the following equation:

$$i = \frac{RT}{zFR_{ct}} \qquad \text{Eq. 8}$$

where z is the number of transferred electrons. The linearized Arrhenius equation for the electrochemical process can be presented as:

$$\ln(i) = lnA - \frac{E_a}{RT} \qquad \text{Eq. 9}$$

where A is a constant and E_a is the activation energy of the reaction. Therefore, $\ln(T/R_{ct})=f(1/T)$ plot can be used to determine the activation energy from EIS measurements performed at different temperatures [58, 59]. E_a value calculated from the obtained line slope (Figure 6b) for the blank solution is 18.6 kJ/mol, which is comparable to the values reported by other authors [60–63]. Activation energy determined for the solution containing inhibitor is 34.3 kJ/mol, which proves that the presence of Na_2HFol in the solution results in the activation energy increase.

3.4. UV-VIS spectroscopy

Analysis of folic acid molecular structure suggests that it might be unstable in water solution, especially at higher temperatures, but also on contact with UV-light and oxygen [64]. The formation of new compounds and a significant decrease in Na_2HFol concentration as a result of its decomposition can affect the adsorption process and make the obtained results invalid. To investigate the potential chemical changes in Na_2HFol solution, a series of UV-VIS measurements was performed. The obtained spectra (Figure 7) consist of two absorption bands with the maxima at approximately 300 and 350 nm wavelengths and are similar to the spectra of water solutions containing $HFol^{2-}$ anions reported in the literature [65]. Maximum absorbance values are listed in Table 6 for clarity. Spectrum A was measured just after the preparation of 4 mM solution of Na_2HFol. The solution was then divided between four beakers. The solution in the first beaker was heated to 80°C and stirred for 1 hour, and spectrum B was measured. The absorbance value was almost unchanged, therefore it can be stated that no significant changes occurred in the inhibitor structure as a result of heating. Further three beakers were left for 24 hours at room temperature, and measurements were carried out. In the first of them (spectrum C) was only the solution of Na_2HFol. Absorbance values are slightly lower, but comparable to those obtained for spectra A and B, hence the changes observed after short-time immersion are not significant in the context of adsorption process. The second (spectrum D) contained a copper coupon and no important difference in absorbance was observed in comparison to spectrum C. The last beaker (spectrum E) contained a copper coupon and 3.5% NaCl. It is worth noticing that the solution was visibly darker than the others. While the absorbance value for λ=300 nm is similar to that measured in spectra C and D, the value for λ=350 nm is lower and the absorption band is deformed, which corresponds to the color change and can be attributed to the interaction (for instance the formation of coordination compound) between some folate molecules and Cu^{2+} ions unchained from the metal surface during the corrosion process caused by the presence of chlorides.

3.5. Surface analysis

3.5.1. Microscopic photographs

The inhibiting action of sodium folate can be observed even with unaided eye (see Supplementary material) and in microscopic photographs (Figure 8). On the surface of copper specimen after polishing (1A) some scratches from emery paper are visible. In the case of the specimen immersed in the solution without Na_2HFol (2A), orange, red and green corrosion product are present. Changes observed on the surface of inhibited one (3A) are noticeably smaller, which proves that the corrosion process is slower.

3.5.2. Scanning electron microscopy

SEM images of copper specimens are presented in Figure 8. In comparison to the polished copper specimen (1B), the surface of specimen immersed in 3.5% NaCl solution (2B) is severely damaged and corrosion products are visible. The specimen immersed in the solution containing Na_2HFol (3B) is also corroded (structural changes such as corrosion centers can be observed) but significantly less than the uninhibited one, several scratches from emery paper

are still visible.

3.5.3. Energy-dispersive X-Ray Spectroscopy

EDX spectroscopy was used to determine the elemental composition of the copper surface after polishing and immersion in the solution with or without inhibitor. The obtained results are presented in Table 7. Copper content in immersed specimens is lower than in the freshly polished one, whereas oxygen and chlorine content is higher as a result of the corrosion products formation. However, the content of chlorine and oxygen is significantly lower for the inhibited specimen than for uninhibited, which confirms that the larger amount of copper chlorides and oxides was formed in the inhibitor absence (the corrosion rate was higher). Carbon content in the polished specimen and in the one exposed to the solution without inhibitor is similar. Noticeably higher value reported for the specimen immersed in the solution with Na_2HFol may be attributed to the presence of sodium folate molecules on the metal surface.

3.6. Conclusions

Thorough analysis of the results described above leads to the following conclusions:

- Sodium folate acts as an effective, mixed-type (with predominant cathodic character), barrier corrosion inhibitor for copper in 3.5% NaCl.
- Inhibitor efficiency increases with concentration.
- During first 12 hours of immersion, inhibitor efficiency increases, however, efficiency values after long-term (20 days) immersion are significantly lower due to the protective corrosion products layer formation on the copper surface in uninhibited solution.
- Langmuir adsorption model showed the best fit for the obtained data, calculated Gibbs free energy of adsorption indicates mixed-type or physical adsorption character, which is in agreement with the temperature effect on inhibitor efficiency (temperature increase results in efficiency decrease).
- Inhibitor presence in the solution results in the activation energy increase.
- No significant chemical changes were observed due to heating or 24 h storage of inhibitor solution, however the interaction between folate anions and Cu^{2+} ions migrating to the solution from the corroding surface was reported.
- In the presence of inhibitor electrode surface is in significantly better condition than after immersion in uninhibited solution.

Taking into account the promising results presented and discussed in this paper, further studies may be carried out to apply the inhibitor in other environments and to find potential synergistic effects between sodium folate and other (especially green) copper corrosion inhibitors.

3.7. References

[1] U. S. Geological Survey, Mineral Commodity Summaries 2023: U. S. Geological Survey, 2023. https://doi.org/10.3133/mcs2023.

[2] A. Fateh, M. Aliofkhazraei, A.R. Rezvanian, Review of corrosive environments for copper and its corrosion inhibitors, Arabian Journal of Chemistry 13 (2020) 481–544. https://doi.org/10.1016/j.arabjc.2017.05.021.

[3] G. Kear, B.D. Barker, F.C. Walsh, Electrochemical corrosion of unalloyed copper in chloride media--a critical review, Corros Sci 46 (2004) 109–135. https://doi.org/10.1016/S0010-938X(02)00257-3.

[4] El-Taib Heakal F., Haruyama S., Impedance studies of the inhibitive effect of benzotriazole on the corrosion of copper in sodium chloride medium, Corros Sci 20 (1980) 887–898.

[5] Y. Qiang, S. Zhang, S. Yan, X. Zou, S. Chen, Three indazole derivatives as corrosion inhibitors of copper in a neutral chloride solution, Corros Sci 126 (2017) 295–304. https://doi.org/10.1016/j.corsci.2017.07.012.

[6] M. Finšgar, D. Kek Merl, An electrochemical, long-term immersion, and XPS study of 2-

mercaptobenzothiazole as a copper corrosion inhibitor in chloride solution, Corros Sci 83 (2014) 164–175. https://doi.org/10.1016/j.corsci.2014.02.016.
[7] F. Zucchi, G. Trabanelli, M. Fonsati, Tetrazole derivatives as corrosion inhibiotrs for copper in chloride solutions, Corros Sci 38 (1996) 2019-2029.
[8] Z. Khiati, A.A. Othman, M. Sanchez-Moreno, M.C. Bernard, S. Joiret, E.M.M. Sutter, V. Vivier, Corrosion inhibition of copper in neutral chloride media by a novel derivative of 1,2,4-triazole, Corros Sci 53 (2011) 3092–3099. https://doi.org/10.1016/j.corsci.2011.05.042.
[9] M. Finšgar, A. Lesar, A. Kokalj, I. Milošev, A comparative electrochemical and quantum chemical calculation study of BTAH and BTAOH as copper corrosion inhibitors in near neutral chloride solution, Electrochim Acta 53 (2008) 8287–8297. https://doi.org/10.1016/j.electacta.2008.06.061.
[10] C.U. Dueke Eze, N.A. Madueke, N.B. Iroha, N.J. Maduelosi, L.A. Nnanna, V.C. Anadebe, A.A. Chokor, Adsorption and inhibition study of N-(5-methoxy-2-hydroxybenzylidene) isonicotinohydrazide Schiff base on copper corrosion in 3.5% NaCl, Egyptian Journal of Petroleum 31 (2022) 31–37. https://doi.org/10.1016/j.ejpe.2022.05.001.
[11] Y. Zhou, S. Xu, L. Guo, S. Zhang, H. Lu, Y. Gong, F. Gao, Evaluating two new Schiff bases synthesized on the inhibition of corrosion of copper in NaCl solutions, RSC Adv 5 (2015) 14804–14813. https://doi.org/10.1039/c4ra14449j.
[12] M. Scendo, The influence of adenine on corrosion of copper in chloride solutions, Corros Sci 50 (2008) 2070–2077. https://doi.org/10.1016/j.corsci.2008.04.007.
[13] K.M. Ismail, Evaluation of cysteine as environmentally friendly corrosion inhibitor for copper in neutral and acidic chloride solutions, Electrochim Acta 52 (2007) 7811–7819. https://doi.org/10.1016/j.electacta.2007.02.053.
[14] C. Li, X. yu Guo, S. Shen, P. Song, T. Xu, Y. Wen, H.F. Yang, Adsorption and corrosion inhibition of phytic acid calcium on the copper surface in 3wt% NaCl solution, Corros Sci 83 (2014) 147–154. https://doi.org/10.1016/j.corsci.2014.02.001.
[15] S. Mo, L.J. Li, H.Q. Luo, N.B. Li, An example of green copper corrosion inhibitors derived from flavor and medicine: Vanillin and isoniazid, J Mol Liq 242 (2017) 822–830. https://doi.org/10.1016/j.molliq.2017.07.081.
[16] M. Zdravković, V. Grekulović, J. Suljagić, D. Stanković, S. Savić, M. Radovanović, U. Stamenković, 2023. Influence of blackberry leaf extract on the copper corrosion behaviour in 0.5 M NaCl. Bioelectrochemistry 151, 108401. https://doi.org/10.1016/j.bioelechem.2023.108401.
[17] P. Refait, C. Rahal, M. Masmoudi, 2020. Corrosion inhibition of copper in 0.5 M NaCl solutions by aqueous and hydrolysis acid extracts of olive leaf. Journal of Electroanalytical Chemistry 859, 113834. https://doi.org/10.1016/j.jelechem.2020.113834.
[18] M.H. Fekri, F. Omidali, M.M. Alemnezhad, A. Ghaffarinejad, 2022. Turnip peel extract as green corrosion bio-inhibitor for copper in 3.5% NaCl solution. Mater Chem Phys 286, 126150. https://doi.org/10.1016/j.matchemphys.2022.126150.
[19] Oukhrib R., El Ibrahimi B., Bourzi H., El Mouaden K., Jmiai A., El Issami S., Bammou L., Bazzi L., Quantum chemical calculations and corrosion inhibition efficiency of biopolymer “chitosan” on copper surface in 3%NaCl, Journal of Materials and Environmental Sciences 8 (2017) 195–208.
[20] V. Grudić, I. Bošković, A. Gezović, Inhibition of copper corrosion in NaCl solution by propolis extract, Chem Biochem Eng Q 32 (2018) 299–305. https://doi.org/10.15255/CABEQ.2018.1357.
[21] N. Velazquez-Torres, H. Martinez, J. Porcayo-Calderon, E. Vazquez-Velez, J.G. Gonzalez-Rodriguez, L. Martinez-Gomez, Use of an amide-type corrosion inhibitor synthesized from the coffee bagasse oil on the corrosion of Cu in NaCl, Green Chem Lett Rev 11 (2018) 1–11. https://doi.org/10.1080/17518253.2017.1404645.
[22] F. Scaglione, G. Panzavolta, Folate, folic acid and 5-methyltetrahydrofolate are not the same thing, Xenobiotica 44 (2014) 480–488. https://doi.org/10.3109/00498254.2013.845705.
[23] Folate and folic acid, in: Vitamin and Mineral Requirements in Human Nutrition. Second Edition., World Health Organization and Food and Agriculture Organization of the United Nations, 2004: pp. 289–300.
[24] K.S. Crider, L.B. Bailey, R.J. Berry, Folic acid food fortification-its history, effect, concerns, and future directions, Nutrients 3 (2011) 370–384. https://doi.org/10.3390/nu3030370.
[25] R. Debowska, K. Rogiewicz, T. Iwanenko, M. Kruszewski, I. Eris, Folsäure (Folacin)-Neue Neue Anwendungsmöglichkeiten eines kosmetischen Wirkstoffes Folic Acid (Folacin)-New Application of a Cosmetic Ingredient, Kosmetische Medizin 3 (2005) 16–22.
[26] S. Mohapatra, S.K. Mallick, T.K. Maiti, S.K. Ghosh, P. Pramanik, 2007. Synthesis of highly stable folic acid conjugated magnetite nanoparticles for targeting cancer cells. Nanotechnology 18, 385102. https://doi.org/10.1088/0957-4484/18/38/385102.
[27] G. Ali Mansoori, K.S. Brandenburg, A. Shakeri-Zadeh, A comparative study of two folate-conjugated gold nanoparticles for cancer nanotechnology applications, Cancers (Basel) 2 (2010) 1911–1928. https://doi.org/10.3390/cancers2041911.
[28] E. Roger, S. Kalscheuer, A. Kirtane, B.R. Guru, A.E. Grill, J. Whittum-Hudson, J. Panyam, Folic acid

functionalized nanoparticles for enhanced oral drug delivery, Mol Pharm 9 (2012) 2103–2110. https://doi.org/10.1021/mp2005388.
[29] A. Narmani, M. Rezvani, B. Farhood, P. Darkhor, J. Mohammadnejad, B. Amini, S. Refahi, N. Abdi Goushbolagh, Folic acid functionalized nanoparticles as pharmaceutical carriers in drug delivery systems, Drug Dev Res 80 (2019) 404–424. https://doi.org/10.1002/ddr.21545.
[30] I. Sekine, Y. Nakahata, H. Tanabe, The corrosion inhibition of mild steel by ascorbic and folic acids, Corros Sci 28 (1988) 987–1001.
[31] D.S. Kalyani, S.S. Rao, 2014. Chemical Science Review and Letters Effect of Various Factors on Corrosion Inhibition of Carbon Steel Using a Phosphonate-Based Inhibitor System. Che Sci Rev Lett 2, CS19204398.
[32] K.J. Orie, A.O. James, O. Akaranta, The Corrosion Inhibition of Mild Steel in 0.5m Phosphoric Acid and Crown Cork in Water By Folic Acid , International Journal of Science and Research 4 (2015) 1380–1385.
[33] A.M. Farhan, N.A. Hikmat, N.K. Nemer, K.E. Ahmed, A Study Of Corrosion Inhibition Of Low Carbon Steel In Washing Water Of Crude Oil Solution In The Presence Of Folic Acid, Baghdad Science Journal 11 (2014) 1171–1179.
[34] E. Hamed, Studies of the corrosion inhibition of copper in Na2SO4 solution using polarization and electrochemical impedance spectroscopy, Mater Chem Phys 121 (2010) 70–76. https://doi.org/10.1016/j.matchemphys.2009.12.044.
[35] A. Dehghani, G. Bahlakeh, B. Ramezanzadeh, A detailed electrochemical/theoretical exploration of the aqueous Chinese gooseberry fruit shell extract as a green and cheap corrosion inhibitor for mild steel in acidic solution, J Mol Liq 282 (2019) 366–384. https://doi.org/10.1016/j.molliq.2019.03.011.
[36] D. Li, P. Zhang, X. Guo, X. Zhao, Y. Xu, The inhibition of mild steel corrosion in 0.5 M H2SO4 solution by radish leaf extract, RSC Adv 9 (2019) 40997–41009. https://doi.org/10.1039/c9ra04218k.
[37] E.A. Noor, The impact of some factors on the inhibitory action of Radish seeds aqueous extract for mild steel corrosion in 1M H2SO4 solution, Mater Chem Phys 131 (2011) 160–169. https://doi.org/10.1016/j.matchemphys.2011.08.001.
[38] E. Bottari, A. D'Ambrosio, G. De Tommaso, M.R. Festa, M. Iuliano, M. Meschino, Solubility of folic acid and protonation of folate in NaCl at different concentrations, even in physiological solution, Analyst 146 (2021) 2339–2347. https://doi.org/10.1039/d1an00013f.
[39] F. Mansfeld, Fundamental aspects of the polarization resistance technique-the early days, Journal of Solid State Electrochemistry 13 (2009) 515–520. https://doi.org/10.1007/s10008-008-0652-x.
[40] ASTM G59-97 Standard Test Method for Conducting Potentiodynamic Polarization Resistance Measurements.
[41] A. Popova, M. Christov, A. Vasilev, Mono- and dicationic benzothiazolic quaternary ammonium bromides as mild steel corrosion inhibitors. Part II: Electrochemical impedance and polarisation resistance results, Corros Sci 53 (2011) 1770–1777. https://doi.org/10.1016/j.corsci.2011.01.055.
[42] ASTM G5-13 Standard Reference Test Method for Making Potentiodynamic Anodic Polarization Measurements.
[43] ASTM G1-90 Standard Practice for Preparing, Cleaning, and Evaluating Corrosion Test Specimens.
[44] C. Jing, Z. Wang, Y. Gong, H. Huang, Y. Ma, H. Xie, H. Li, S. Zhang, F. Gao, Photo and thermally stable branched corrosion inhibitors containing two benzotriazole groups for copper in 3.5 wt% sodium chloride solution, Corros Sci 138 (2018) 353–371. https://doi.org/10.1016/j.corsci.2018.04.027.
[45] D. Wang, B. Xiang, Y. Liang, S. Song, C. Liu, Corrosion control of copper in 3.5 wt.% NaCl Solution by Domperidone: Experimental and Theoretical Study, Corros Sci 85 (2014) 77–86. https://doi.org/10.1016/j.corsci.2014.04.002.
[46] H. Lgaz, S.K. Saha, H.S. Lee, N. Kang, F.Z. Thari, K. Karrouchi, R. Salghi, K. Bougrin, I.H. Ali, 2021. Corrosion inhibition properties of thiazolidinedione derivatives for copper in 3.5 wt.% nacl medium. Metals (Basel) 11, 1861. https://doi.org/10.3390/met11111861.
[47] L. Feng, S. Zhang, Y. Qiang, Y. Xu, L. Guo, L.H. Madkour, S. Chen, 2018. Experimental and theoretical investigation of thiazolyl blue as a corrosion inhibitor for copper in neutral sodium chloride solution. Materials 11, 1042. https://doi.org/10.3390/ma11061042.
[48] S. Pareek, D. Jain, S. Hussain, A. Biswas, R. Shrivastava, S.K. Parida, H.K. Kisan, H. Lgaz, I.M. Chung, D. Behera, A new insight into corrosion inhibition mechanism of copper in aerated 3.5 wt.% NaCl solution by eco-friendly Imidazopyrimidine Dye: experimental and theoretical approach, Chemical Engineering Journal 358 (2019) 725–742. https://doi.org/10.1016/j.cej.2018.08.079.
[49] K.F. Khaled, M.N.H. Hamed, K.M. Abdel-Azim, N.S. Abdelshafi, Inhibition of copper corrosion in 3.5% NaCl solutions by a new pyrimidine derivative: Electrochemical and computer simulation techniques, Journal of Solid State Electrochemistry 15 (2011) 663–673. https://doi.org/10.1007/s10008-010-1110-0.
[50] E. McCafferty, Validation of corrosion rates measured by the Tafel extrapolation method, Corros Sci 47

(2005) 3202–3215. https://doi.org/10.1016/j.corsci.2005.05.046.
[51] V. Sastri, Adsorption in Corrosion Inhibition, in: Green Corrosion Inhibitors, John Wiley & Sons, Hoboken, 2011: pp. 103–136.
[52] A. Miralrio, A.E. Vázquez, 2020. Plant extracts as green corrosion inhibitors for different metal surfaces and corrosive media: A review. Processes 8, 942. https://doi.org/10.3390/PR8080942.
[53] J.T. Nwabanne, V. Nwoye Okafor, Adsorption and Thermodynamics Study of the Inhibition of Corrosion of Mild Steel in H2SO4 Medium Using Vernonia amygdalina, Journal of Minerals and Materials Characterization and Engineering 11 (2012) 885–890.
[54] E.E. Ebenso, H. Alemu, S.A. Umoren, I.B. Obot, Inhibition of Mild Steel Corrosion in Sulphuric Acid Using Alizarin Yellow GG Dye and Synergistic Iodide Additive, Int J Electrochem Sci 3 (2008) 1325–1339.
[55] Y. Boughoues, M. Benamira, L. Messaadia, N. Ribouh, 2020. Adsorption and corrosion inhibition performance of some environmental friendly organic inhibitors for mild steel in HCl solution via experimental and theoretical study. Colloids Surf A Physicochem Eng Asp 593, 124610. https://doi.org/10.1016/j.colsurfa.2020.124610.
[56] A. Kokalj, 2022. Corrosion inhibitors: physisorbed or chemisorbed? Corros Sci 196, 109939. https://doi.org/10.1016/j.corsci.2021.109939.
[57] O. Sanni, A.P.I. Popoola, O.S.I. Fayomi, 2019. Temperature Effect, Activation Energies and Adsorption Studies of Waste Material as Stainless Steel Corrosion Inhibitor in Sulphuric Acid 0.5 M. J Bio Tribocorros 5, 88. https://doi.org/10.1007/s40735-019-0280-2.
[58] K. Zhang, L. Wang, Z. Hu, F. Cheng, J. Chen, 2014. Ultrasmall Li2S nanoparticles anchored in graphene nanosheets for high-energy lithium-ion batteries. Sci Rep 4, 6467. https://doi.org/10.1038/srep06467.
[59] J. Ryl, J. Wysocka, M. Cieslik, H. Gerengi, T. Ossowski, S. Krakowiak, P. Niedzialkowski, Understanding the origin of high corrosion inhibition efficiency of bee products towards aluminium alloys in alkaline environments, Electrochim Acta 304 (2019) 263–274. https://doi.org/10.1016/j.electacta.2019.03.012.
[60] N. Benzbiria, S. Echihi, M.E. Belghiti, A. Thoume, A. Elmakssoudi, A. Zarrouk, M. Zertoubi, M. Azzi, Novel synthetized benzodiazepine as efficient corrosion inhibitor for copper in 3.5% NaCl solution, Mater Today Proc 37 (2021) 3932-3939. https://doi.org/10.1016/j.matpr.2020.09.030.
[61] M. Askari, A. Ghaffarinejad, Copper corrosion prevention in 3.5% NaCl solution by Spartium junceum petals extract as an eco-friendly bio-inhibitor: kinetic and thermodynamic studies, Analytical Sciences (2023) 1967-1979. https://doi.org/10.1007/s44211-023-00407-4.
[62] H. Huang, B. Li, X. Zheng, J. Fan, M. Gong, 2022. Influence of Anions on the Corrosion Inhibition Effect of Imidazolium Based Ionic Liquids for Copper in 3.5 % NaCl Solution. Int J Electrochem Sci 17, 220344. https://doi.org/10.20964/2022.03.32.
[63] H. Tian, W. Li, B. Hou, Electrochemical and Theoretical Investigation of Triazole Derivatives as Corrosion Inhibitors for Copper in 3.5% NaCl Solution, International Journal of Electrochemical Science 8 (2013) 8513–8529.
[64] A.M. Gazzali, M. Lobry, L. Colombeau, S. Acherar, H. Azaïs, S. Mordon, P. Arnoux, F. Baros, R. Vanderesse, C. Frochot, Stability of folic acid under several parameters, European Journal of Pharmaceutical Sciences 93 (2016) 419–430. https://doi.org/10.1016/j.ejps.2016.08.045.
[65] V. Magri, M. Rocha, C.S. De Matos, P.A.D. Petersen, F. Leroux, H. Petrilli, V.R.L. Constantino, 2022. Folic acid and sodium folate salts: Thermal behavior and spectroscopic (IR, Raman, and solid-state 13C NMR) characterization. Spectrochim. Acta A Mol. Biomol. Spectrosc 273, 120981 https://doi.org/10.1016/j.saa.2022.120981

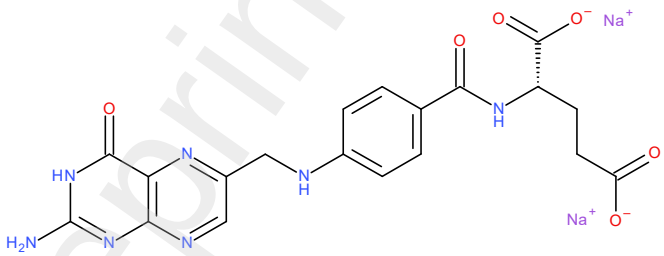

Figure 1. Sodium folate structure.

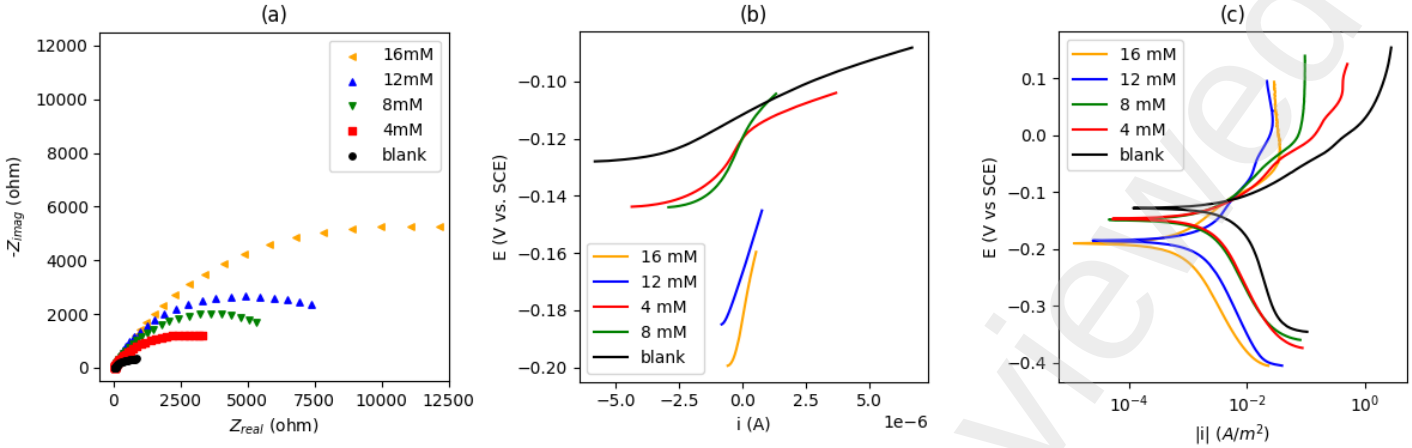

Figure 2. (a) EIS spectra in Nyquist projection (b) linear polarization curves (c) potentiodynamic polarization curves obtained for different concentrations of inhibitor.

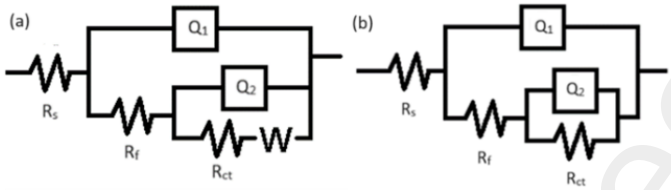

Figure 3. Electrical equivalent circuits used for EIS data fitting.

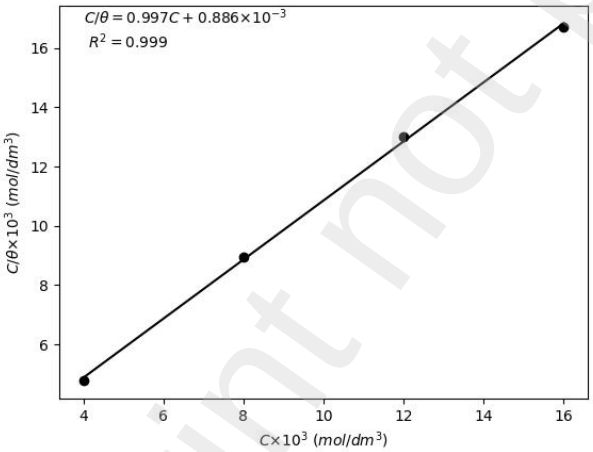

Figure 4. Graphical representation of Langmuir adsorption isotherm.

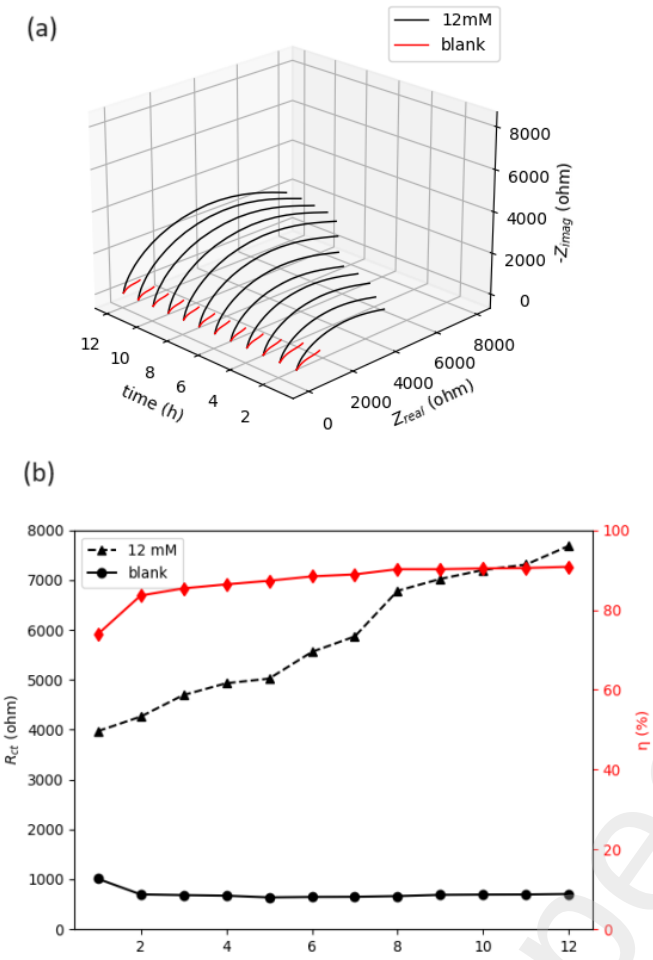

Figure 5. (a) EIS spectra obtained for inhibited and uninhibited system during 12h of immersion (b) charge transfer resistance (R_{ct}) and inhibitor efficiency (η) changes in time.

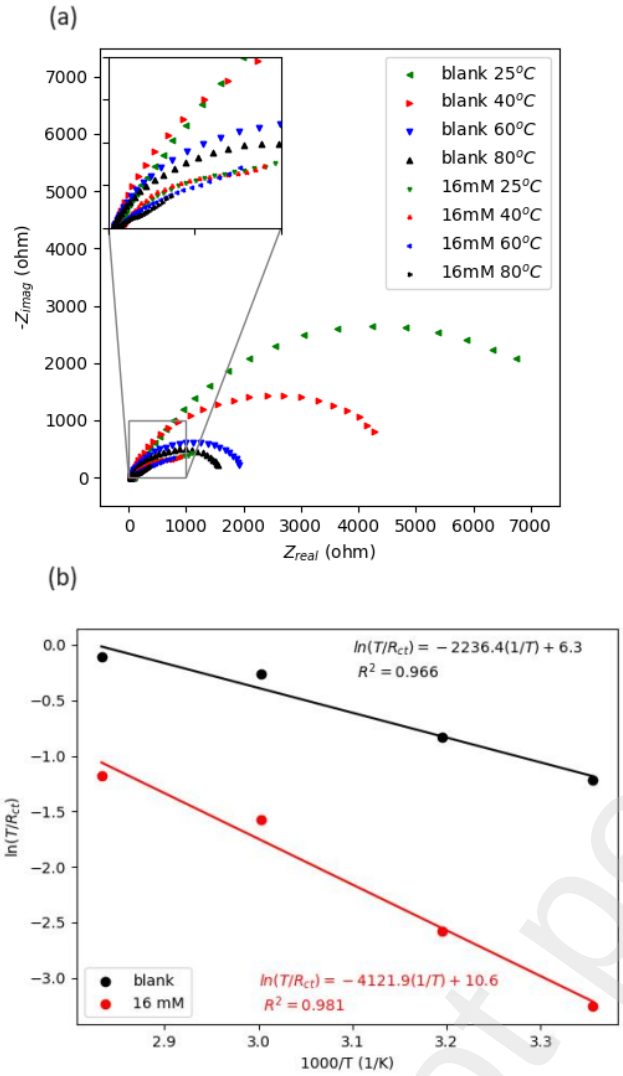

Figure 6. (a) EIS spectra obtained for inhibited and uninhibited system at different temperatures (b) Arrhenius plots.

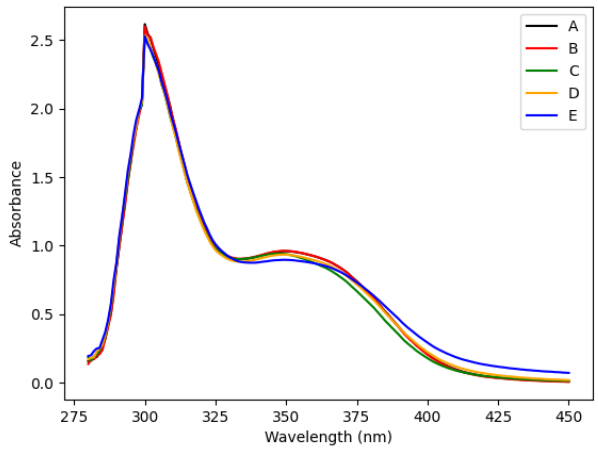

Figure 7. UV-VIS spectra.

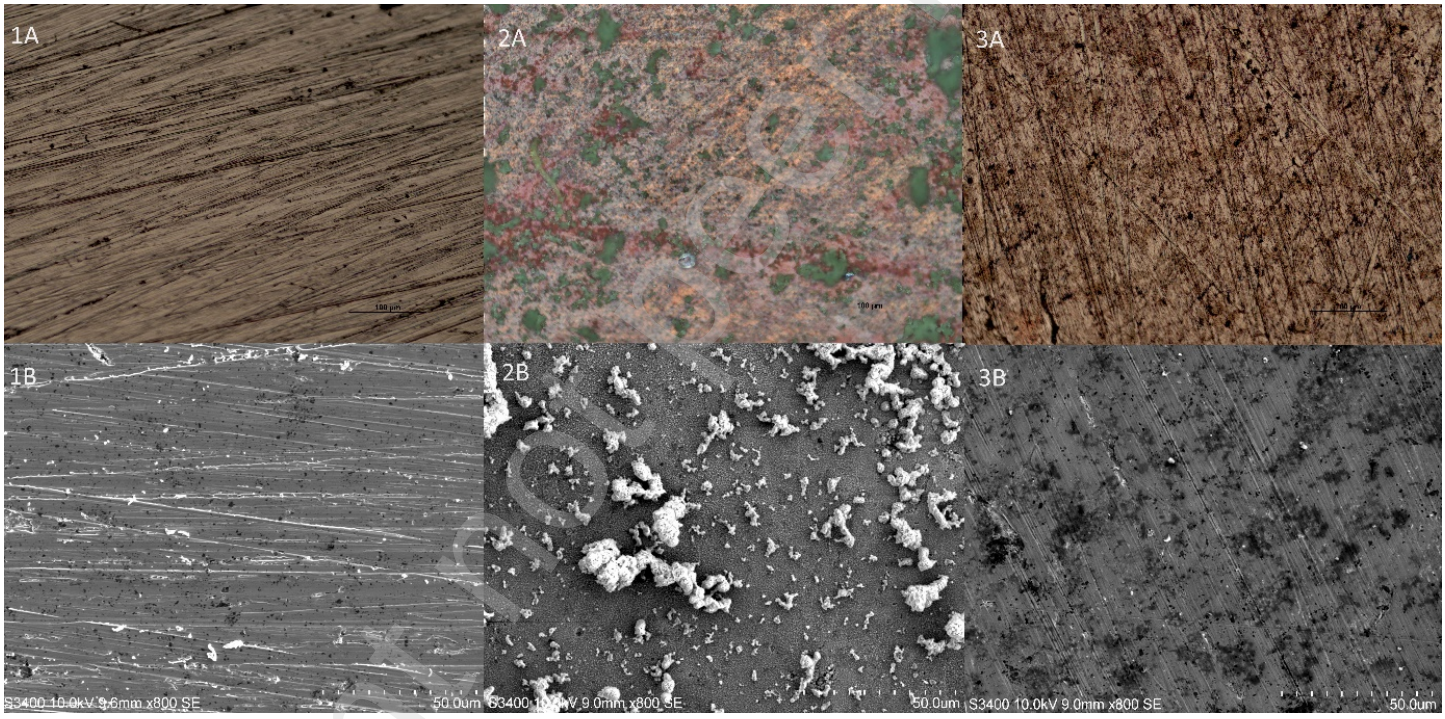

Figure 8. Microscopic photographs (A) and SEM images (B) of copper specimens after polishing with emery paper (1) and after 7 days of immersion in the solution without (2) and with (3) sodium folate.

C (mM)	R_s (ohm)	Q_1 ($S \cdot s^n$)	n_1	R_f (ohm)	Q_2 ($S \cdot s^n$)	n_2	R_{ct} (ohm)	W ($S \cdot s^{0.5}$)	$\chi^2 \cdot 10^4$	η (%)

0	54.44	$1.25\cdot10^{-4}$	0.58	36	$2.71\cdot10^{-4}$	0.69	798	$3.76\cdot10^{-3}$	2.79	-
4	53.86	$3.26\cdot10^{-5}$	0.79	594	$1.58\cdot10^{-4}$	0.40	4971	$1.60\cdot10^{-3}$	8.77	83.9
8	53.81	$2.36\cdot10^{-5}$	0.83	777	$8.55\cdot10^{-5}$	0.48	7574	-	3.38	89.5
12	53.67	$2.29\cdot10^{-5}$	0.85	1939	$8.33\cdot10^{-5}$	0.40	10270	-	2.07	92.2
16	52.94	$1.99\cdot10^{-5}$	0.81	2141	$3.38\cdot10^{-5}$	0.51	18840	-	2.30	95.8

Table 1. EIS data obtained for different inhibitor concentrations.

Linear polarization resistance			Weight-loss method			
C (mM)	R_p (kohm)	η (%)	C (mM)	Δm (mg)	Δm/S (mg/cm^2)	η (%)
0	1.731	-	0	40.70(±0.33)	1.881(±0.021)	-
4	12.58	86.2	4	27.50(±0.22)	1.269(±0.014)	32.5(±1.5)
8	19.38	91.0	8	19.20(±0.27)	0.887(±0.014)	52.8(±1.3)
12	26.56	93.5	12	15.70(±0.37)	0.727(±0.018)	61.3(±1.4)
16	50.12	96.5	16	11.90(±0.29)	0.551(±0.014)	70.7(±1.1)

Table 2. Results obtained with linear polarization resistance and weight-loss method.

Adsorption isotherm	Linearized equation	R^2
Langmuir	$\frac{C}{\theta} = \frac{1}{K} + C$	0.999
Freundlich	$log\theta = nlogC + logK$	0.992
Temkin	$\theta = lnC + K$	0.990
El-Awady	$log\frac{\theta}{1-\theta} = \text{ylogC} + \text{K' where } K' = K^y$	0.923
Flory-Huggins	$log\frac{\theta}{C} = blog(1-\theta) + logK$	0.908
Frumkin	$\log\left(C\frac{\theta}{1-\theta}\right) = 2\alpha\theta + 2.303logK$	0.996

Table 3. Examined adsorption isotherm models with obtained determination coefficients (n, y, α are constants).

C (mM)	t (h)	R_s (ohm)	Q_1 (S·s^n)	n_1	R_f (ohm)	Q_2 (S·s^n)	n_2	R_{ct} (ohm)	W (S·s$^{0.5}$)	$\chi^2\cdot10^4$	η (%)
0	1	55.97	$5.34\cdot10^{-5}$	0.67	34	$2.47\cdot10^{-4}$	0.57	1011	$2{,}63\cdot10^{-3}$	6.11	-
	4	55.37	$3.81\cdot10^{-4}$	0.51	87	$1.27\cdot10^{-4}$	0.71	672	$3.18\cdot10^{-3}$	1.83	-
	8	57.2	$2.87\cdot10^{-4}$	0.55	52	$2.14\cdot10^{-4}$	0.69	644	$3.57\cdot10^{-3}$	1.95	-
	12	57.0	$1.73\cdot10^{-4}$	0.59	43	$2.47\cdot10^{-4}$	0.69	706	$3.80\cdot10^{-3}$	0.99	-
12	1	57.83	$2.82\cdot10^{-5}$	0.85	1659	$1.83\cdot10^{-4}$	0.50	3868	-	2.33	73.9
	4	56.97	$2.30\cdot10^{-5}$	0.88	2194	$1.49\cdot10^{-4}$	0.47	4930	-	2.37	86.4
	8	57.29	$1.81\cdot10^{-5}$	0.90	3167	$1.08\cdot10^{-4}$	0.43	6783	-	2.61	90.2
	12	57.4	$1.62\cdot10^{-5}$	0.90	2612	$7.10\cdot10^{-4}$	0.46	7687	-	2.66	90.8

Table 4. Selected EIS data obtained for inhibited and uninhibited system during 12h immersion.

C (mM)	T (°C)	R_s (ohm)	Q_1 ($S \cdot s^n$)	n_1	R_f (ohm)	Q_2 ($S \cdot s^n$)	n_2	R_{ct} (ohm)	W ($S \cdot s^{0.5}$)	$\chi^2 \cdot 10^4$	η (%)
0	25	55.97	$5.34 \cdot 10^{-5}$	0.67	34	$2.47 \cdot 10^{-4}$	0.57	1011	$2{,}63 \cdot 10^{-3}$	6.11	-
	40	56.54	$7.79 \cdot 10^{-5}$	0.65	39	$2.36 \cdot 10^{-4}$	0.72	719	$2.99 \cdot 10^{-3}$	6.35	-
	60	48.37	$1.92 \cdot 10^{-3}$	0.22	7	$1.26 \cdot 10^{-3}$	0.58	432	$3.54 \cdot 10^{-4}$	9.44	-
	80	46.49	$2.95 \cdot 10^{-6}$	0.92	6	$1.30 \cdot 10^{-3}$	0.44	391	$1.81 \cdot 10^{-3}$	44.4	-
16	25	57.40	$1.89 \cdot 10^{-6}$	0.87	1793	$5.37 \cdot 10^{-5}$	0.66	7749	-	2.29	87.0
	40	40.35	$2.11 \cdot 10^{-5}$	0.87	1075	$8.60 \cdot 10^{-5}$	0.54	4108	-	2.89	82.5
	60	32.30	$3.01 \cdot 10^{-5}$	0.84	647	$1.53 \cdot 10^{-4}$	0.53	1605	-	9.34	73.0
	80	27.28	$4.02 \cdot 10^{-5}$	0.81	592	$1.92 \cdot 10^{-4}$	0.62	1146	-	3.10	65.9

Table 5. EIS data obtained for inhibited and uninhibited system at different temperatures.

Spectrum	A_{300}	A_{350}
A	2.616	0.959
B	2.6	0.962
C	2.534	0.942
D	2.533	0.934
E	2.528	0.896

Table 6. Absorbance (A) values measured for wavelength 300 and 350 nm.

Element	Elemental composition of the specimen (wt. %)		
	After polishing	With inhibitor	Without inhibitor
Cu	97.252(±0.013)	93.66(±0.38)	78.78(±0.42)
O	0.957(±0.060)	1.95(±0.08)	10.12(±0.13)
Cl	-	0.26(±0.06)	8.16(±0.22)
C	1.790(±0.068)	3.27(±0.07)	1.50(±0.13)
N	-	0.86(±0.10)	0.70(±0.15)
K	-	-	0.74(±0.10)

Table 7. Elemental composition of copper specimens determined with EDX spectroscopy.

Glossary

Field-specific terms used in the article are listed and shortly described below. Terms that are commonly used in physical chemistry and materials science (e.g. “adsorption” or “corrosion”) were ommited.

Corrosion inhibitor	A substance that added to a corrosive medium in small amounts causes a significant corrosion rate decrease
Barrier inhibitor	Corrosion inhibitor that adsorbs on the metal surface and forms a protecting film, which limits mass exchange processes to and from the surface
Anodic inhibitor	Corrosion inhibitor that added to the solution significantly shifts up the potential
Cathodic inhibitor	Corrosion inhibitor that added to the solution significantly shifts down the potential
Mixed-type inhibitor	Corrosion inhibitor that added to the solution does not cause potential changes or the observed potential changes are small
Working electrode	An electrode on which the studied process occurs
Reference electrode	An electrode with defined and maintained potential, which is used as a reference for measurement by the working electrode
Auxiliary electrode	An electrode used in three-electrode electrochemical cell to allow the current flow in the system and to stabilize an interfacial potential
Inhibitor efficiency	Value that quantifies the inhibiting action by comparing the corrosion rates with and without inhibitor (expressed in percents)
Open circuit potential	Potential value measured when the current does not flow through the system
Charge-transfer resistance	Value that expresses the difficulty of electron transfer process
Double layer capacitance	Value that provides a characteristics of the electrical double layer on the electrode surface
Tafel region	A part of the polarization curve (potential E vs. current in logarithmic scale log|i|) that is linear (it follows Tafel’s law)
Tafel extrapolation	A method for determination of an exchange current based on Tafel’s law